Hogan, J., & Kristiansen, K. U. (2017). On the regularization of impact without collision: the Painlevé paradox and compliance. *Proceedings of the Royal Society A: Mathematical, Physical and Engineering Sciences*, *473*, [20160773]. https://doi.org/10.1098/rspa.2016.0773

PROCEEDINGS A

rspa.royalsocietypublishing.org

Research

Cite this article: Hogan SJ, Uldall Kristiansen K. 2017 On the regularization of impact without collision: the Painlevé paradox and compliance. *Proc. R. Soc. A* **473**: 20160773. http://dx.doi.org/10.1098/rspa.2016.0773

Received: 14 October 2016
Accepted: 18 May 2017

Subject Areas:
applied mathematics, mechanics

Keywords:
Painlevé paradox, impact without collision, compliance, regularization

Author for correspondence:
S. J. Hogan
e-mail: s.j.hogan@bristol.ac.uk

THE ROYAL SOCIETY
PUBLISHING

On the regularization of impact without collision: the Painlevé paradox and compliance

S. J. Hogan[1] and K. Uldall Kristiansen[2]

[1]Department of Engineering Mathematics, University of Bristol, Bristol BS8 1UB, UK
[2]Department of Applied Mathematics and Computer Science, Technical University of Denmark, 2800 Kongens Lyngby, Denmark

SH, 0000-0001-6012-6527

We consider the problem of a rigid body, subject to a unilateral constraint, in the presence of Coulomb friction. We regularize the problem by assuming compliance (with both stiffness and damping) at the point of contact, for a general class of normal reaction forces. Using a rigorous mathematical approach, we recover impact without collision (IWC) in both the inconsistent and the indeterminate Painlevé paradoxes, in the latter case giving an exact formula for conditions that separate IWC and lift-off. We solve the problem for arbitrary values of the compliance damping and give explicit asymptotic expressions in the limiting cases of small and large damping, all for a large class of rigid bodies.

1. Introduction

In mechanics, in problems with unilateral constraints in the presence of friction, the rigid-body assumption can result in the governing equations having multiple solutions (the *indeterminate* case) or no solutions (the *inconsistent* case). The classical example of Painlevé [1–3], consisting of a slender rod slipping[1] along a rough surface (figure 1), is the simplest and most studied example of these phenomena, now known collectively as *Painlevé paradoxes* [5–8]. Such paradoxes can occur at physically realistic parameter values in many important engineering systems [9–15].

[1]We prefer to avoid describing this phase of the motion as *sliding* because we will be using ideas from piecewise smooth systems [4], where sliding has exactly the opposite meaning.

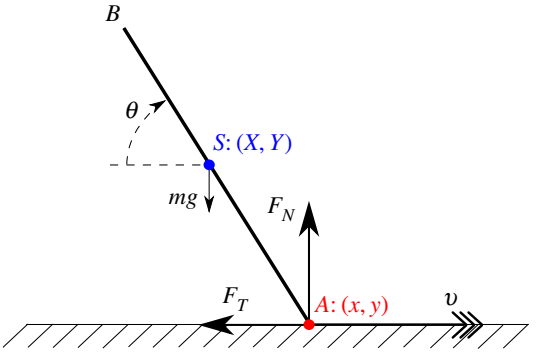

Figure 1. The classical Painlevé problem.

When a system has no *consistent* solution, it cannot remain in that state. Lecornu [16] proposed a jump in vertical velocity to escape an inconsistent, horizontal velocity, state. This jump has been called *impact without collision* (IWC) [17], *tangential impact* [18] or *dynamic jamming* [13]. Experimental evidence of IWC is given in [15]. IWC can be incorporated into the rigid-body formulation [19,20] by considering the equations of motion in terms of the normal impulse, rather than time.

Génot & Brogliato [17] considered the dynamics around a critical point, corresponding to zero vertical acceleration of the end of the rod. They proved that, when starting in a consistent state, the rod must stop slipping before reaching the critical point. In particular, paradoxical situations cannot be reached after a period of slipping.

One way to address the Painlevé paradox is to *regularize* the rigid-body formalism. Physically, this often corresponds to assuming some sort of compliance at the contact point A, typically thought of as a spring, with stiffness (and sometimes damping) that tends to the rigid body model in a suitable limit. Mathematically, very little rigorous work has been done on how IWC and Painlevé paradoxes can be regularized. Dupont & Yamajako [21] treated the problem as a slow–fast system, as we will do. They explored the fast time-scale dynamics, which is unstable for the Painlevé paradoxes. Song *et al.* [22] established conditions under which these dynamics can be stabilized. Le Suan An [23] considered a system with bilateral constraints and showed qualitatively the presence of a regularized IWC as a jump in vertical velocity from a compliance model with diverging stiffness. Zhao *et al.* [24] considered the example in figure 1 and regularized the equations by assuming a compliance that consisted of an *undamped* spring. They estimated, as a function of the stiffness, the orders of magnitude of the time taken in each phase of the (regularized) IWC. Another type of regularization was considered by Neimark & Smirnova [25], who assumed that the normal and tangential reactions took (different) finite times to adjust.

In this paper, we present the first rigorous analysis of the regularized rigid-body formalism, in the presence of compliance with both stiffness *and* damping. We recover IWC in both the inconsistent and the indeterminate cases, and in the latter case, we present a formula for conditions that separate IWC and lift-off. We solve the problem for arbitrary values of the compliance damping and give explicit asymptotic expressions in the limiting cases of small and large damping. Our results apply directly to a general class of rigid bodies. Our approach is similar to that used in [26,27] to understand the forward problem in piecewise smooth (PWS) systems in the presence of a twofold.

The paper is organized as follows. In §2, we introduce the problem, outline some of the main results known to date and include compliance. In §3, we give a summary of our main results, theorems 3.1 and 3.2, before presenting their derivation in §§4 and 5. We discuss our results in §6 and outline our conclusion in §7.

2. Classical Painlevé problem

Consider a rigid rod AB, slipping on a rough horizontal surface, as depicted in figure 1.

The rod has mass m, length $2l$, the moment of inertia of the rod about its centre of mass S is given by I and its centre of mass coincides with its centre of gravity. The point S has coordinates (X, Y) relative to an inertial frame of reference (x, y) fixed in the rough surface. The rod makes an angle θ with respect to the horizontal, with θ increasing in a clockwise direction. At A, the rod experiences a contact force $(-F_T, F_N)$, which opposes the motion. The dynamics of the rod is then governed by the following equations:

$$\left.\begin{aligned} m\ddot{X} &= -F_T, \\ m\ddot{Y} &= -mg + F_N \\ \text{and} \qquad I\ddot{\theta} &= -l(\cos\theta F_N - \sin\theta F_T), \end{aligned}\right\} \tag{2.1}$$

where g is the acceleration due to gravity, plus the unilateral constraint $y \geq 0$.

The coordinates (X, Y) and (x, y) are related geometrically as follows:

$$x = X + l\cos\theta \quad \text{and} \quad y = Y - l\sin\theta. \tag{2.2}$$

We now adopt the scalings $(X, Y) = l(\tilde{X}, \tilde{Y}), (x, y) = l(\tilde{x}, \tilde{y}), (F_T, F_N) = mg(\tilde{F}_T, \tilde{F}_N), \ t = 1/\omega\tilde{t}$, $\alpha = ml^2/I$, where $\omega^2 = g/l$. For a uniform rod, $I = \frac{1}{3}ml^2$, and so $\alpha = 3$ in this case.

Then for general α, (2.1) and (2.2) can be combined to become, on dropping the tildes,

$$\left.\begin{aligned} \ddot{x} &= -\dot{\theta}^2\cos\theta + \alpha\sin\theta\cos\theta F_N - (1 + \alpha\sin^2\theta)F_T, \\ \ddot{y} &= -1 + \dot{\theta}^2\sin\theta + (1 + \alpha\cos^2\theta)F_N - \alpha\sin\theta\cos\theta F_T \\ \text{and} \qquad \ddot{\theta} &= -\alpha(\cos\theta F_N - \sin\theta F_T). \end{aligned}\right\} \tag{2.3}$$

To proceed, we need to determine the relationship between F_N and F_T. We assume Coulomb friction between the rod and the surface. Hence, when $\dot{x} \neq 0$, we set

$$F_T = \mu\,\mathrm{sign}(\dot{x})F_N, \tag{2.4}$$

where μ is the coefficient of friction. By substituting (2.4) into (2.3), we obtain two sets of governing equations for the motion, depending on the sign of $\dot{x}$, as follows:

$$\left.\begin{aligned} &\dot{x} = v, \quad \dot{v} = a(\theta, \phi) + q_\pm(\theta)F_N, \quad \dot{y} = w, \\ &\dot{w} = b(\theta, \phi) + p_\pm(\theta)F_N, \quad \dot{\theta} = \phi \quad \text{and} \quad \dot{\phi} = c_\pm(\theta)F_N, \end{aligned}\right\} \tag{2.5}$$

where the variables v, w, ϕ denote velocities in the x, y, θ directions, respectively, and

$$\left.\begin{aligned} &a(\theta, \phi) = -\phi^2\cos\theta, \quad q_\pm(\theta) = \alpha\sin\theta\cos\theta \mp \mu(1 + \alpha\sin^2\theta), \\ &b(\theta, \phi) = -1 + \phi^2\sin\theta, \quad p_\pm(\theta) = 1 + \alpha\cos^2\theta \mp \mu\alpha\sin\theta\cos\theta \\ \text{and} \qquad &c_\pm(\theta) = -\alpha(\cos\theta \mp \mu\sin\theta) \end{aligned}\right\} \tag{2.6}$$

for the configuration in figure 1. The suffices $\pm$ correspond to $\dot{x} = v \gtrless 0$, respectively.

Suppose F_N is known. Then system (2.5) is a Filippov system [4]. Hence, we obtain a well-defined forward flow when $\dot{x} = v = 0$ and

$$a(\theta, \phi) + q_+(\theta)F_N < 0 < a(\theta, \phi) + q_-(\theta)F_N, \tag{2.7}$$

where $\dot{v}$ in $(2.5)_\pm$ for $v \gtrless 0$ both oppose $v = 0$, by using the Filippov vector-field [4]. Simple computations give the following:

Proposition 2.1. *The Filippov vector-field, within the subset of the switching manifold* $\Sigma : \dot{x} = v = 0$ *where* (2.7) *holds, is given by*

$$\left.\begin{aligned} &\dot{y} = w, \quad \dot{w} = b(\theta,\phi) + S_w(\theta)F_N, \\ &\dot{\theta} = \phi \quad \text{and} \quad \dot{\phi} = S_\phi(\theta)F_N, \end{aligned}\right\} \tag{2.8}$$

where

$$\left.\begin{aligned} S_w(\theta) &= \frac{q_-(\theta)}{q_-(\theta)-q_+(\theta)}p_+(\theta) - \frac{q_+(\theta)}{q_-(\theta)-q_+(\theta)}p_-(\theta) = \frac{1+\alpha}{1+\alpha\sin^2\theta} \\ \text{and} \qquad S_\phi(\theta) &= \frac{q_-(\theta)}{q_-(\theta)-q_+(\theta)}c_+(\theta) - \frac{q_+(\theta)}{q_-(\theta)-q_+(\theta)}c_-(\theta) = -\frac{\alpha\cos\theta}{1+\alpha\sin^2\theta}. \end{aligned}\right\} \tag{2.9}$$

Remark 2.2. Our results hold for mechanical systems with different $q_\pm$, $p_\pm$ and $c_\pm$ in (2.6) and even dependency on several angles $\theta \in \mathbb{T}^d$, e.g. the two-link mechanism of Zhao *et al.* [15]. As expected, S_w and S_ϕ in (2.9) are independent of μ, even for general $q_\pm$, $p_\pm$ and $c_\pm$.

To solve (2.5) and (2.8), we need to determine F_N. The constraint-based method leads to the Painlevé paradox. The compliance-based method is the subject of this paper.

(a) Constraint-based method

In order that the constraint $y = 0$ be maintained, $\ddot{y}(= \dot{w})$ and F_N form a complementarity pair given by

$$\dot{w} \geq 0, \quad F_N \geq 0, \quad F_N \cdot \dot{w} = 0. \tag{2.10}$$

Note that $F_N \geq 0$ since the rough surface can only push, not pull, the rod. Then for general motion of the rod, F_N and y satisfy the complementarity conditions

$$0 \leq F_N \perp y \geq 0. \tag{2.11}$$

In other words, at most one of F_N and y can be positive.

For the system shown in figure 1, the Painlevé paradox occurs when $v > 0$ and $\theta \in (0, \pi/2)$, provided $p_+(\theta) < 0$, as follows. From the fourth equation in (2.5), we can see that b is the free acceleration of the end of the rod. Therefore, if $b > 0$, lift-off is always possible when $y = 0$, $w = 0$. But if $b < 0$, in equilibrium we would expect a forcing term F_N to maintain the rod on $y = 0$. From $\dot{w} = 0$, we obtain

$$F_N = -\frac{b}{p_+} \tag{2.12}$$

since $v > 0$. If $p_+ > 0$, which is always true for $\theta \in (\pi/2, \pi)$, then $F_N \geq 0$, in line with (2.11). But if $p_+ < 0$, which can happen if $\theta \in (0, \pi/2)$, then $F_N < 0$ in (2.12). Then, F_N is in an *inconsistent* (or *non-existent*) mode. On the other hand, if $b > 0$ and $p_+ < 0$, then $F_N > 0$ in (2.12). At the same time, lift-off is also possible from $y = 0$ and hence F_N is in an *indeterminate* (or *non-unique*) mode. It is straightforward to show that $p_+(\theta) < 0$ requires

$$\mu > \mu_P(\alpha) \equiv \frac{2}{\alpha}\sqrt{1+\alpha}. \tag{2.13}$$

Then, the Painlevé paradox can occur for $\theta \in (\theta_1, \theta_2)$, where

$$\left.\begin{aligned} \theta_1(\mu,\alpha) &= \arctan\tfrac{1}{2}(\mu\alpha - \sqrt{\mu^2\alpha^2 - 4(1+\alpha)}) \\ \text{and} \qquad \theta_2(\mu,\alpha) &= \arctan\tfrac{1}{2}(\mu\alpha + \sqrt{\mu^2\alpha^2 - 4(1+\alpha)}). \end{aligned}\right\} \tag{2.14}$$

For a uniform rod with $\alpha = 3$, we have $\mu_P(3) = 4/3$. For $\alpha = 3$ and $\mu = 1.4$, the dynamics can be summarized[2] in the (θ, ϕ)-plane, as in figure 2. Along $\theta = \theta_1, \theta_2$, we have $p_+(\theta) = 0$. These lines intersect the curve $b(\theta, \phi) = 0$ at four points: $\phi^\pm_{1,2} = \pm\sqrt{\csc\theta_{1,2}}$. Génot & Brogliato [17] showed that the point $P : (\theta, \phi) = (\theta_1, \sqrt{\csc\theta_1})$ is the most important and analysed the local dynamics around

[2]Compare with fig. 2 of Génot & Brogliato [17], where the authors plot the *unscaled* angular velocity $\omega\phi$ versus θ, for the case $g = 9.8\,\mathrm{ms}^{-2}$, $l = 1\,\mathrm{m}$.

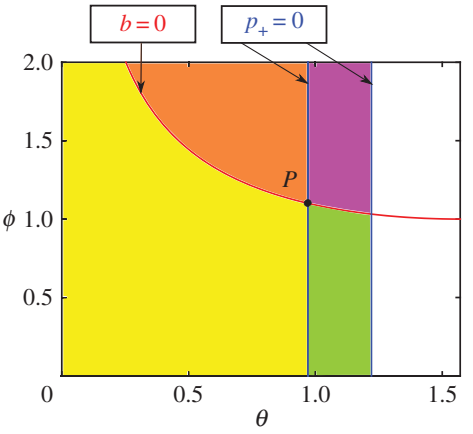

Figure 2. The (θ, ϕ)-plane for the classical Painlevé problem of figure 1, for $\alpha = 3$ and $\mu = 1.4$. The point P has coordinates $(\theta_1, \sqrt{\csc\theta_1})$, where θ_1 is given in (2.14). In the first quadrant centred on P, we have $b > 0$, $p_+ < 0$, so the dynamics is indeterminate (non-unique). In the second quadrant, $b > 0$, $p_+ > 0$ and the rod lifts off the rough surface. In the third quadrant, $b < 0$, $p_+ > 0$ and the rod moves (slips) along the surface. Here, Génot & Brogliato [17] showed that the dynamics cannot cross $p_+ = 0$ unless also $b = 0$. In the fourth quadrant, $b < 0$, $p_+ < 0$ and the dynamics is inconsistent (non-existent). Even though the constraint $y = 0$ is satisfied, there exists no positive value of F_N, contradicting (2.11).

it. The rigid body equations (2.1) are unable to resolve the dynamics in the third and fourth quadrants. So, we regularize these equations using compliance.

(b) Compliance-based method

We assume that there is compliance at the point A between the rod and the surface, when they are in contact (figure 1). Following [21,28], we assume that there are small excursions into $y < 0$. Then we require that the nonnegative normal force $F_N(y, w)$ is a PWS function of (y, w):

$$F_N(y,w) = [f(y,w)] \equiv \begin{cases} 0 & \text{for } y > 0 \\ \max\{f(y,w), 0\} & \text{for } y \le 0, \end{cases} \tag{2.15}$$

where the operation $[\cdot]$ is defined by the last equality and $f(y, w)$ is assumed to be a smooth function of (y, w) satisfying $\partial_y f < 0, \partial_w f < 0$. The quantities $-\partial_y f(0,0)$ and $-\partial_w f(0,0)$ represent a (scaled) spring constant and damping coefficient, respectively. We are interested in the case when the compliance is very large, so we introduce a small parameter ϵ as follows:

$$\partial_y f(0,0) = -\epsilon^{-2} \quad \text{and} \quad \partial_w f(0,0) = -\epsilon^{-1}\delta. \tag{2.16}$$

This choice of scaling [21,28] ensures that the critical damping coefficient ($\delta_{\text{crit}} = 2$ in the classical Painlevé problem) is independent of ϵ. Our analysis can handle any f of the form $f(y, w) = \epsilon^{-1} h(\epsilon^{-1} y, w)$ with

$$h(\hat{y}, w) = -\hat{y} - \delta w + \mathcal{O}((\hat{y} + w)^2). \tag{2.17}$$

But, to obtain our quantitative results, we truncate (2.17) and consider the linear function

$$h(\hat{y}, w) = -\hat{y} - \delta w, \tag{2.18}$$

so that

$$F_N(y,w) = \epsilon^{-1}[-\epsilon^{-1} y - \delta w]. \tag{2.19}$$

In what follows, the first equation in (2.5) will play no role, so we drop it from now on. Then we combine the remaining five equations in (2.5) with (2.15) and (2.16) to give the following set

of governing equations that we will use in the sequel:

$$\left.\begin{aligned} &\dot{y} = w, \quad \dot{w} = b(\theta,\phi) + p_{\pm}(\theta)\epsilon^{-1}[-\epsilon^{-1}y - \delta w],\\ &\dot{\theta} = \phi, \quad \dot{\phi} = c_{\pm}(\theta)\epsilon^{-1}[-\epsilon^{-1}y - \delta w]\\ \text{and}\quad &\dot{v} = a(\theta,\phi) + q_{\pm}(\theta)\epsilon^{-1}[-\epsilon^{-1}y - \delta w], \end{aligned}\right\} \tag{2.20}$$

For $\epsilon > 0$, this is a well-defined Filippov system. The slipping region (2.7) and the Filippov vector-field (2.8) are obtained by replacing F_N in these expressions with the square bracket $\epsilon^{-1}[-\epsilon^{-1}y - \delta w]$ (see also lemma 4.10).

3. Main results

We now present the main results of our paper, theorems 3.1 and 3.2. Theorem 3.1 shows that, if the rod starts in the fourth quadrant of figure 2, it undergoes (regularized) IWC for a time of $\mathcal{O}(\epsilon \ln \epsilon^{-1})$. The same theorem also gives expressions for the resulting vertical velocity of the rod in terms of the compliance damping and initial horizontal velocity and orientation of the rod.

Theorem 3.1. *Consider an initial condition*

$$(y, w, \theta, \phi, v) = (0, \mathcal{O}(\epsilon), \theta_0, \phi_0, v_0), \quad v_0 > 0, \tag{3.1}$$

within the region of inconsistency (non-existence) where

$$p_+(\theta_0) < 0, \quad b(\theta_0, \phi_0) < 0, \tag{3.2}$$

and $q_+(\theta_0) < 0$, $q_-(\theta_0) > 0$, $a \neq 0$. *Then the forward flow of (3.1) under (2.20) returns to* $\{(y, w, \theta, \phi, v) \,|y = 0\}$ *after a time* $\mathcal{O}(\epsilon \ln \epsilon^{-1})$ *with*

$$\left.\begin{aligned} &w = e(\delta,\theta_0)v_0 + o(1), \quad \theta = \theta_0 + o(1),\\ \text{and}\quad &\phi = \phi_0 + \left\{-\frac{c_+(\theta_0)}{q_+(\theta_0)} + \frac{S_\phi(\theta_0)}{S_w(\theta_0)}\left(e(\delta,\theta_0) + \frac{p_+(\theta_0)}{q_+(\theta_0)}\right)\right\} v_0 + o(1), \quad v = o(1), \end{aligned}\right\} \tag{3.3}$$

as $\epsilon \to 0$. *During this time* $y = \mathcal{O}(\epsilon)$, $w = \mathcal{O}(1)$ *so that* $F_N = \mathcal{O}(\epsilon^{-1})$. *The function* $e(\delta, \theta_0)$, *given in (4.30), is smooth and monotonic in* δ *and has the following asymptotic expansions*:

$$e(\delta,\theta_0) = \frac{p_-(\theta_0) - p_+(\theta_0)}{q_-(\theta_0)p_+(\theta_0) - q_+(\theta_0)p_-(\theta_0)}\delta^{-2}(1 + \mathcal{O}(\delta^{-2}\ln\delta^{-1})) \quad \text{for } \delta \gg 1 \tag{3.4}$$

and

$$\begin{aligned} e(\delta,\theta_0) = &\sqrt{\frac{p_+(\theta_0)(p_-(\theta_0) - p_+(\theta_0))}{q_+(\theta_0)(q_-(\theta_0) - q_+(\theta_0))}}\\ &\times \left(1 - \frac{\sqrt{S_w(\theta_0)}}{2}\left(\pi - \arctan\left(\sqrt{-\frac{S_w(\theta_0)}{p_+(\theta_0)}}\right)\right)\delta + \mathcal{O}(\delta^2)\right) \quad \text{for } \delta \ll 1. \end{aligned} \tag{3.5}$$

Theorem 3.2 is similar to theorem 3.1, but now the rod starts in the first quadrant of figure 2. This theorem also gives an exact formula for initial conditions that separate (regularized) IWC and lift-off.

Theorem 3.2. *Consider an initial condition*

$$(y, w, \theta, \phi, v) = (0, \epsilon w_{10}, \theta_0, \phi_0, v_0) \quad \text{and} \quad w_{10} < w_{1*} \equiv -\lambda_-(\theta_0)\frac{b(\theta_0,\phi_0)}{p_+(\theta_0)} < 0, \tag{3.6}$$

with λ_- *defined in (4.6), within the region of indeterminacy (non-uniqueness) where*

$$p_+(\theta_0) < 0 \quad \text{and} \quad b(\theta_0,\phi_0) > 0, \tag{3.7}$$

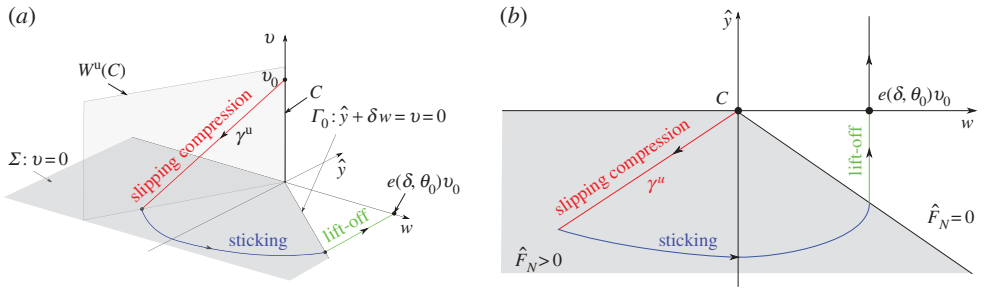

Figure 3. The limit $\epsilon \longrightarrow 0$ shown using (a) the $(w, \hat{y}, v)$-variables and (b) a projection onto the $(w, \hat{y})$-plane. The *slipping compression* phase, shown in red, where $\hat{y}$, w and $v > 0$ all decrease, is described geometrically by an unstable manifold γ^u (4.5) of a critical set C, given in (4.4). It ends on the switching manifold Σ. The subsequent *sticking* phase (in blue) is described by Filippov [4]. It ends along Γ_0. From there, the *lift-off* phase (in green) occurs and we return to $\hat{y} = 0$. In both figures, the grey region is where $\hat{F}_N > 0$.

and $q_+(\theta_0) < 0$, $q_-(\theta_0) > 0$, $a \neq 0$. *Then the conclusions of theorem* 3.1, *including expressions* (3.3)–(3.5), *still hold true as* $\epsilon \to 0$. *For* $w_{10} > w_{1*}$ *lift-off occurs directly after a time* $\mathcal{O}(\epsilon)$ *with* $w = \mathcal{O}(\epsilon)$. *During this period,* $y = \mathcal{O}(\epsilon^2)$, *so* $F_N = \mathcal{O}(1)$.

Remark 3.3. These two theorems have not appeared before in the literature. In the rigid-body limit ($\epsilon \to 0$), we recover IWC in both cases. Previous authors have not carried out the 'very difficult' calculation [28], performed numerical calculations [6,21] or given a range of estimates for the time of (regularized) IWC in the *absence* of damping [24]. We give exact and asymptotic expressions for key quantities as well as providing a geometric interpretation of our results, for a large class of rigid bodies, in the presence of a large class of normal forces, as well as giving a precise estimate for the time of (regularized) IWC, all in the presence of both stiffness and damping. Note that we are not attempting to describe all the dynamics around P. There is a canard connecting the third quadrant with the first, and the analysis of it is exceedingly complicated [29] due to fast oscillatory terms. Instead, we follow [24] and consider that the rod dynamics starts in a configuration with $p_+(\theta_0) < 0$.

4. Proof of theorem 3.1: impact without collision in the inconsistent case

The proof of theorem 3.1 is divided into three phases, illustrated in figure 3. These phases are a generalization of the phases of IWC in its rigid-body formulation [15].

— Slipping compression (§4b): During this phase, y, w and v all decrease. The dynamics follow an unstable manifold γ^u of a set of critical points C, given in (4.4) below, as $\epsilon \to 0$. Along γ^u the normal force $F_N = \mathcal{O}(\epsilon^{-1})$ and v will therefore quickly decrease to 0. Mathematically, this part is complicated by the fact that the initial condition (3.1) belongs to the critical set C as $\epsilon \to 0$.
— Sticking (§4c): Since $F_N = \mathcal{O}(\epsilon^{-1})$ and $q_+ q_- < 0$, the rod will stick with $v \equiv 0$. During this phase, $\ddot{y} = \dot{w} > 0$ and eventually sticking ends with $F_N = 0$ as $\epsilon \to 0$.
— Lift-off (§4d): In the final phase $F_N = 0$, lift-off occurs and the system eventually returns to $y = 0$.

(a) Slow–fast setting: initial scaling

Before we consider the first phase of IWC, we apply the scaling

$$y = \epsilon \hat{y}, \tag{4.1}$$

also used in [21,28], which brings the two terms in (2.19) to the same order. Now let

$$\hat{F}_N(\hat{y}, w) \equiv \epsilon F_N(\epsilon\hat{y}, w) = [-\hat{y} - \delta w]. \tag{4.2}$$

Equations (2.20) then read

$$\left.\begin{aligned} \hat{y}' &= w, \quad w' = \epsilon b(\theta,\phi) + p_\pm(\theta)\hat{F}_N(\hat{y}, w),\\ \theta' &= \epsilon\phi, \quad \phi' = c_\pm(\theta)\hat{F}_N(\hat{y}, w)\\ \text{and}\qquad v' &= \epsilon a(\theta,\phi) + q_\pm(\theta)\hat{F}_N(\hat{y}, w), \end{aligned}\right\} \tag{4.3}$$

with respect to the *fast time* $\tau = \epsilon^{-1}t$, where $()' = \mathrm{d}/\mathrm{d}\tau$. This is a slow–fast system in non-standard form [28]. Only θ is truly slow whereas $(\hat{y}, w, \phi, v)$ are all fast. But the set of critical points

$$C = \{(\hat{y}, w, \theta, \phi, v) | \hat{y} = 0, w = 0\}, \tag{4.4}$$

for $\epsilon = 0$ is just three-dimensional. System (4.3) is PWS [26,27]. We now show that $(4.3)_+$ contains stable and unstable manifolds $\gamma^{\mathrm{s,u}}$ when the equivalent rigid-body equations exhibit a Painlevé paradox, when $p_+(\theta_0) < 0$. The saddle structure of C within the fourth quadrant has been recognized before [21–23].

Proposition 4.1. *Consider system* $(4.3)_+$ *with* $\epsilon = 0$. *Then for* $p_+(\theta_0) < 0$, *there exist smooth stable and unstable sets* $\gamma^{\mathrm{s,u}}(\theta_0, \phi_0, v_0)$, *respectively, of* $(\hat{y}, w, \theta, \phi, v) = (0, 0, \theta_0, \phi_0, v_0) \in C$ *contained within* $\hat{F}_N \geq 0$ *given by*

$$\gamma^{\mathrm{s,u}}(\theta_0,\phi_0,v_0) = \left\{(\hat{y}, w, \theta, \phi, v) |\ w = \lambda_\mp\hat{y},\ \theta = \theta_0,\ \phi = \phi_0 - c_+(\theta_0)\lambda_\mp^{-1}[1 + \delta\lambda_\mp]\hat{y},\right.$$
$$\left. v = v_0 + \frac{q_+(\theta_0)}{p_+(\theta_0)}\lambda_\mp(\theta_0)\hat{y},\ \hat{y} \leq 0\right\}, \tag{4.5}$$

with $\lambda_\mp(\theta_0) \lessgtr 0$ *given in* (4.6).

Proof. Consider the smooth system, $(4.3)_{\hat{F}_N = -\hat{y} - \delta w}$, obtained from (4.3) by setting $\hat{F}_N = -\hat{y} - \delta w$ with $\epsilon = 0$. The linearization of $(4.3)_{\hat{F}_N = -\hat{y} - \delta w}$ about a point in C with $\epsilon = 0$ then only has two non-zero eigenvalues:

$$\lambda_\pm(\theta) = -\frac{\delta p_+(\theta)}{2} \pm \frac{1}{2}\sqrt{\delta^2 p_+(\theta)^2 - 4p_+(\theta)}, \tag{4.6}$$

satisfying

$$\lambda_\pm^2 = -p_+(\theta)(1 + \delta\lambda_\pm). \tag{4.7}$$

For $p_+(\theta) < 0$, we have $\lambda_- < 0 < \lambda_+$. The eigenvectors associated with $\lambda_\pm$ are $v_\pm = (1, \lambda_\pm, 0, (c_+/p_+(\theta))\lambda_\pm, (q_+/p_+(\theta))\lambda_\pm)^{\mathrm{T}}$. Therefore, the smooth system $(4.3)_{\hat{F}_N = -\hat{y} - \delta w, \epsilon = 0}$ has a (stable and unstable) manifold $\gamma^{\mathrm{s,u}}$ tangent to $v_\mp$ at $(\hat{y}, w, \theta, \phi, v) = (0, 0, \theta_0, \phi_0, v_0)$. But then for $\hat{y} \leq 0$, we have $\hat{F}_N(\hat{y}, \lambda_\pm\hat{y}) = -(1 + \delta\lambda_\pm)\hat{y} = (\lambda_\pm^2/p_+(\theta))\hat{y} \geq 0$, by (4.7). Hence, the restrictions of $\gamma^{\mathrm{s,u}}$ in (4.5) to $\hat{y} \leq 0$ are (stable and unstable) sets of C for the PWS system $(4.3)_{\hat{F}_N = [-\hat{y} - \delta w], \epsilon = 0}$. ∎

Remark 4.2. For the smooth system $(4.3)_{\hat{F}_N = -\hat{y} - \delta w}$, the critical manifold C perturbs by Fenichel's theory [30–32] to a smooth slow manifold C_ϵ, being C^∞ $\mathcal{O}(\epsilon)$-close to C for $0 < \epsilon \ll 1$. A simple calculation shows that $C_\epsilon : \hat{y} = \epsilon(b(\theta,\phi)/p_+(\theta))(1 + \mathcal{O}(\epsilon)), w = \mathcal{O}(\epsilon^2)$. Since $b(\theta,\phi) < 0$ in this case, $C_\epsilon \subset \{\hat{y} > 0\}$ for ϵ sufficiently small. Therefore, the manifold C_ϵ is only invariant for the smooth system $(4.3)_{\hat{F}_N = -\hat{y} - \delta w}$. It is an artefact for the PWS system $(4.3)_{\hat{F}_N = [-\hat{y} - \delta w]}$ since the square bracket vanishes for $\hat{y} > 0$, by (2.15).

Remark 4.3. Our arguments are geometrical and rely on hyperbolic methods of dynamical systems theory only. Therefore, the results remain unchanged qualitatively if we replace the piecewise linear $\hat{F}_N$ in (4.2) with the nonlinear version $\hat{F}_N(\hat{y}, w) = [h(\hat{y}, w)]$, where $h(\hat{y}, w) = -\hat{y} - \delta w + \mathcal{O}((\hat{y} + w)^2)$ as in (2.17), having (2.18) as its linearization about $\hat{y} = w = 0$. We would obtain again a saddle-type critical set C with nonlinear (stable and unstable) manifolds $\gamma^{\mathrm{s,u}}$.

Following the initial scaling (4.1) of this section, we now consider the three phases of IWC.

(b) Slipping compression

The first phase of the regularized IWC: *slipping compression* ends on the *switching manifold*

$$\Sigma = \{(\hat{y}, w, \theta, \phi, v) | v = 0\}, \tag{4.8}$$

shown in figure 3*a*. Proposition 4.4 describes the intersection of the forward flow of initial conditions (3.1) with Σ.

Proposition 4.4. *The forward flow of the initial conditions* (3.1) *under* (4.3) *intersects* Σ *in*

$$\gamma^{\mathrm{u}} \cap \Sigma + o(1) \equiv \left\{ (\hat{y}, w, \theta, \phi, v) \in \Sigma \,|\, \hat{y} = -\frac{p_+(\theta_0)}{q_+(\theta_0)\lambda_+(\theta_0)} v_0 + o(1),\ w = -\frac{p_+(\theta_0)}{q_+(\theta_0)} v_0 + o(1), \right.$$
$$\left. \theta = \theta_0 + o(1),\ \phi = \phi_0 - \frac{c_+(\theta_0)}{q_+(\theta_0)} v_0 + o(1) \right\}, \tag{4.9}$$

as $\epsilon \to 0$.

Remark 4.5. The $o(1)$-term in (4.9) is $\mathcal{O}(\epsilon^c)$ for any $c \in (0,1)$ (see also lemma 4.8).

(i) Proof of proposition 4.4

We prove proposition 4.4 using Fenichel's normal form theory [33]. But since $(4.3)_{\hat{F}_N=[-\hat{y}-\delta w]}$ with $v > 0$ is PWS, care must be taken. There are at least two ways to proceed. One way is to consider the smooth system $(4.3)_{\hat{F}_N=-\hat{y}-\delta w}$, then rectify C_ϵ by straightening out its stable and unstable manifolds. Then, $(4.3)_{\hat{F}_N=-\hat{y}-\delta w}$ will be a standard slow–fast system to which Fenichel's normal form theory applies. Subsequently, one would then have to ensure that conclusions based on the smooth $(4.3)_{\hat{F}_N=-\hat{y}-\delta w}$ also extend to the PWS system $(4.3)_{\hat{F}_N=[-\hat{y}-\delta w]}$. One way to do this is to consider the following scaling

$$\kappa_1 : \hat{y} = r_1 \hat{y}_1, \quad w = r_1 w_1, \quad \epsilon = r_1, \tag{4.10}$$

zooming in on C at $\hat{y} = 0, w = 0$. In terms of the original variables, $y = \epsilon^2 \hat{y}_1$, $w = \epsilon w_1$. Both the scalings $(\hat{y}, w)$ and $(\hat{y}_1, w_1)$ have appeared in the literature [6,21,28].

In this paper, we follow another approach (basically reversing the process described above) which works more directly with the PWS system. Therefore, in §4b(ii), we study the scaling (4.10) first. We will show that the $(\hat{y}_1, w_1)$-system contains important geometry of the PWS system (significant, for example, for the separation of initial conditions in theorem 3.2). Then in §4b(iii), we connect the 'small' ($\hat{y} = \mathcal{O}(\epsilon), w = \mathcal{O}(\epsilon)$) described by (4.10) with the 'large' ($\hat{y} = \mathcal{O}(1), w = \mathcal{O}(1)$) in (4.3) by considering coordinates described by the following transformation:

$$\kappa_2 : \hat{y} = -r_2, \quad w = r_2 w_2, \quad \epsilon = r_2 \epsilon_2. \tag{4.11}$$

For $y_1 < 0$, we have the following coordinate change κ_{21} between κ_1 and κ_2:

$$\kappa_{21} : r_2 = -r_1 y_1, \quad w_2 = -w_1 y_1^{-1}, \quad \epsilon_2 = -y_1^{-1}. \tag{4.12}$$

The coordinates in κ_2 (4.11) appear as a *directional chart* obtained by setting $\bar{y} = -1$ in the blowup transformation $(r, \bar{\hat{y}}, \bar{w}, \bar{\epsilon}) \mapsto (\hat{y}, w, \epsilon)$ given by[3]

$$\hat{y} = r\bar{\hat{y}}, \quad w = r\bar{w}, \quad \epsilon = r\bar{\epsilon}, \quad r \geq 0, \quad (\bar{\hat{y}}, \bar{w}, \bar{\epsilon}) \in S^2 = \{(\bar{\hat{y}}, \bar{w}, \bar{\epsilon}) | \bar{\hat{y}}^2 + \bar{w}^2 + \bar{\epsilon}^2 = 1\}. \tag{4.13}$$

[3]More accurately, the chart $\bar{y} = -1$ corresponds to

$$r = r_1\sqrt{1 + \epsilon_1^2 + w_1^2}, \quad \bar{\hat{y}} = -\frac{1}{\sqrt{1 + \epsilon_1^2 + w_1^2}}, \quad \bar{w} = \frac{w_1}{\sqrt{1 + \epsilon_1^2 + w_1^2}} \quad \text{and} \quad \bar{\epsilon} = \frac{\epsilon_1}{\sqrt{1 + \epsilon_1^2 + w_1^2}},$$

with $\bar{\hat{y}}^2 + \bar{w}^2 + \bar{\epsilon}^2 = 1$. See [34] for further details on directional and scaling charts.

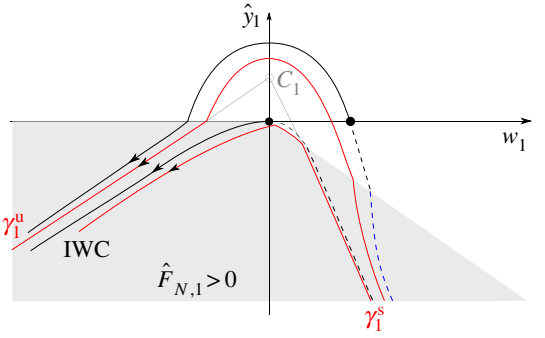

Figure 4. Phase portrait $(4.15)_{\epsilon=0}$ for $b<0$. Theorem 3.1 considers initial conditions on the w_1-axis. The critical set C_1 of $(4.15)_{\hat{F}_{N,1}=-\hat{y}_1-\delta w_1,\epsilon=0}$ is an artefact of the PWS system. The grey region is now where $\hat{F}_{N,1}>0$. Orbit segments outside this region are parabolas. Dashed lines indicate backward orbits, from initial conditions on the w_1-axis. A similar figure appears in [6].

The blowup is chosen so that the zoom in (4.10) coincides with the *scaling chart* obtained by setting $\bar{\epsilon}=1$. The blowup transformation *blows up* C to $\bar{C}$: $r=0$, $(\bar{\tilde{y}},\bar{w},\bar{\epsilon})\in S^2$ a space $(\theta,\phi,v)\in\mathbb{R}^3$ of spheres.[4]

The main advantage of our approach is that in chart κ_2 we can focus on $\bar{C}\cap\{\bar{\tilde{y}}^{-1}\bar{w}>-\delta^{-1},\ \bar{\tilde{y}}<0\}$ (or simply $w_2<\delta^{-1}$ in (4.11)) of $\bar{C}$, the grey area in figure 3, where

$$r^{-1}\hat{F}_N(\hat{y},w)=[-\bar{\tilde{y}}-\delta\bar{w}]=-\bar{\tilde{y}}(1+\delta\bar{\tilde{y}}^{-1}\bar{w})>0, \tag{4.14}$$

and the system will be smooth. This enables us to apply Fenichel's normal form theory [33] there. All the necessary patching for the PWS system is done independently in the scaling chart κ_1.

(ii) Chart κ_1

Let $\hat{F}_{N,1}(\hat{y}_1,w_1)=\epsilon^{-1}\hat{F}_N(\epsilon\hat{y}_1,\epsilon w_1)=[-\hat{y}_1-\delta w_1]$. Then applying chart κ_1 in (4.10) to the non-standard slow–fast system (4.3) gives the following equations:

$$\left.\begin{aligned}&\hat{y}_1'=w_1,\quad w_1'=b(\theta,\phi)+p_+(\theta)\hat{F}_{N,1}(\hat{y}_1,w_1),\\&\theta'=\epsilon\phi,\quad \phi'=\epsilon c_+(\theta)\hat{F}_{N,1}(\hat{y}_1,w_1)\\&\text{and}\qquad\qquad v'=\epsilon(a(\theta,\phi)+q_+(\theta)\hat{F}_{N,1}(\hat{y}_1,w_1)).\end{aligned}\right\} \tag{4.15}$$

The above equation is a slow–fast system in standard form: $(\hat{y}_1,w_1)$ are fast variables, whereas (θ,ϕ,v) are slow variables. By assumption (3.2) of theorem 3.1, $b<0$, $p_+<0$ and so, since $\hat{F}_{N,1}(\hat{y}_1,w_1)\geq 0$, we have $w_1'<0$ in (4.15). Hence, there exists no critical set for the PWS system $(4.15)_{\epsilon=0}$. (The critical set $C_1=\{(\hat{y}_1,w_1,\theta,\phi,v)|\hat{y}_1=b(\theta,\phi)/p_+(\theta),w_1=0\}$ of the *smooth* system $(4.15)_{\hat{F}_{N,1}=-\hat{y}_1-\delta w_1,\epsilon=0}$ lies within $\hat{y}_1>0$. It is therefore an artefact of the PWS system, as illustrated in figure 4 (recall also remark 4.2).)

The unstable manifold γ_1^{u} of C_1 in the smooth system $(4.15)_{\hat{F}_{N,1}=-\hat{y}_1-\delta w_1}$ is given by $w_1=\lambda_+(\theta_0)(\hat{y}_1-b(\theta_0,\phi_0)/p_+(\theta_0))$ and its restriction

$$\gamma_1^{\mathrm{u}}(\theta_0,\phi_0,v_0)=\left\{(\hat{y}_1,w_1,\theta_0,\phi_0,v_0)|\ w_1=\lambda_+(\theta_0)\left(\hat{y}_1-\frac{b(\theta_0,\phi_0)}{p_+(\theta_0)}\right),\ \hat{y}_1\leq 0\right\}, \tag{4.16}$$

[4]Note that (4.13) is not a *blowup* transformation in the sense of Krupa & Szmolyan [35], where geometric blowup is applied in conjunction with desingularization to study loss of hyperbolicity in slow–fast systems. We will not desingularize the vector-field here.

to the subset $\hat{y}_1 \leq 0$, $w_1 \leq 0$ where $\hat{F}_{N,1} \geq 0$, is locally invariant for the PWS system $(4.15)_{\hat{F}_{N,1}=[-\hat{y}_1-\delta w_1]}$. In chart κ_1, initial conditions (3.1) now become

$$(\hat{y}_1, w_1, \theta, \phi, v) = (0, \mathcal{O}(1), \theta_0, \phi_0, v_0). \tag{4.17}$$

Lemma 4.6. *Consider* $\Lambda_1 = \{(\hat{y}_1, w_1, \theta, \phi, v) | \hat{y}_1 = -\nu^{-1}\}$ *with* $\nu > 0$ *small. Then, the forward flow of* (4.17) *under* (4.15) *intersects* Λ_1 *in*

$$z_1(\epsilon) \equiv (-\nu^{-1}, w_{1c}(\nu) + \mathcal{O}(\epsilon), \theta_0 + \mathcal{O}(\epsilon), \phi_0 + \mathcal{O}(\epsilon), v_0 + \mathcal{O}(\epsilon)), \tag{4.18}$$

where $w_{1c}(\nu) = -\lambda_+ \nu^{-1}(1 + o(1))$, $\nu \to 0$.

Proof. Consider the layer problem $(4.15)_{\epsilon=0}$. Since $b < 0$, initial conditions (4.17) with $w_1 > 0$ return to $\hat{y}_1 = 0$ with $w_1 < 0$, see figure 4. Therefore, we consider $w_1(0) \leq 0$ subsequently. From $\lambda_- < 0 < \lambda_+$, it then follows that the solution remains within $\hat{F}_{N,1} > 0$ for $\tau > 0$ for $\epsilon = 0$. The problem is therefore linear. The remaining details of the proof are straightforward and hence omitted. ∎

For $\epsilon > 0$, the variables (ϕ, v) will vary by $\mathcal{O}(1)$-amount as $\hat{y}_1, w_1 \to -\infty$. But the variables (ϕ, v) are fast in (4.3) and slow in (4.15). To describe this transition, we change to chart κ_2.

(iii) Chart κ_2

Writing the non-standard slow–fast PWS system $(4.3)_{\hat{F}_N=[-\hat{y}-\delta w]}$ in chart κ_2, given by (4.11), gives the following smooth (as anticipated by (4.14)) system:

$$\left.\begin{aligned} &\epsilon_2' = \epsilon_2 w_2, \quad w_2' = \epsilon_2 b(\theta, \phi) + p_+(\theta)(1 - \delta w_2) + w_2^2, \\ &\theta' = \epsilon\phi, \quad \phi' = c_+(\theta) r_2 (1 - \delta w_2), \\ &v' = \epsilon a(\theta, \phi) + q_+(\theta) r_2 (1 - \delta w_2) \quad \text{and} \quad r_2' = -r_2 w_2, \end{aligned}\right\} \tag{4.19}$$

on the box $U_2 = \{(\epsilon_2, w_2, \theta, \phi, v, r_2) | \epsilon_2 \in [0, \nu], w_2 \in [-\lambda_+ - \rho, -\lambda_+ + \rho], r_2 \in [0, \nu]\}$, for $\rho > 0$ sufficiently small (so that $w_2 < \delta^{-1}$) and ν as above. Notice that $z_1(\epsilon)$ from (4.18) in chart κ_2 becomes

$$z_2(\epsilon) \equiv \kappa_{21}(z_1(\epsilon)) : \; r_2 = \epsilon \nu^{-1}, \quad w_2 = w_{1c}\nu + \mathcal{O}(\epsilon), \quad \epsilon_2 = \nu, \tag{4.20}$$

using (4.12). Clearly, $z_2(\epsilon) \in \kappa_{21}(\Lambda_1) \subset U_2$, $\kappa_{21}(\Lambda_1)$ being the face of the box U_2 with $\epsilon_2 = \nu$. For simplicity, we will write subsets such as $\{(\epsilon_2, w_2, \theta, \phi, v, r_2) \in U_2 | \cdots\}$ by $\{U_2 | \cdots\}$.

Lemma 4.7. *The set* $M_2 = \{U_2 |\; r_2 = 0, \epsilon_2 = 0, w_2 = -\lambda_+\}$ *is a set of critical points of* (4.19). *Linearization around* M_2 *gives only three non-zero eigenvalues* $-\lambda_+ < 0, \lambda_- - \lambda_+ < 0$, $\lambda_+ > 0$, *and so* M_2 *is of saddle-type. The stable manifold is* $W^{\mathrm{s}}(M_2) = \{U_2 | r_2 = 0\}$ *while the unstable manifold is* $W^{\mathrm{u}}(M_2) = \{U_2 | \epsilon_2 = 0, w_2 = -\lambda_+\}$. *In particular, the one-dimensional unstable manifold* $\gamma_2^{\mathrm{u}}(\theta_0, \phi_0, v_0) \subset W^{\mathrm{u}}(M_2)$ *of the base point* $(\epsilon_2, w_2, \theta, \phi, v, r_2) = (0, 0, \theta_0, \phi_0, v_0, 0) \in M_2$ *is given by*

$$\begin{aligned} \gamma_2^{\mathrm{u}}(\theta_0, \phi_0, v_0) = \Big\{ & U_2 |\; w_2 = -\lambda_+(\theta_0),\; \theta = \theta_0,\; \phi = \phi_0 - \frac{c_+(\theta_0)}{p_+(\theta_0)} \lambda_+(\theta_0) r_2, \\ & v = v_0 - \frac{q_+(\theta_0)}{p_+(\theta_0)} \lambda_+(\theta_0) r_2,\; r_2 \geq 0,\; \epsilon_2 = 0 \Big\}. \end{aligned} \tag{4.21}$$

Proof. The first two statements follow from straightforward calculation. For $\gamma_2^{\mathrm{u}}(\theta_0, \phi_0, v_0)$, we restrict to the invariant set $\epsilon_2 = 0$, $w_2 = -\lambda_+$ and solve the resulting reduced system. ∎

Notice that the set $\gamma_2^{\mathrm{u}}(\theta_0, \phi_0, v_0)$ is just $\gamma^{\mathrm{u}}(\theta_0, \phi_0, v_0)$ in (4.5) written in chart κ_2 for $\epsilon_2 = 0$. Furthermore, note that $z_2(0) \subset W^{\mathrm{s}}(M_2)$. In the subsequent lemma, we follow $z_2(\epsilon) \subset \{\epsilon_2 = \nu\}$ up until $r_2 = \nu$, with ν sufficiently small, by applying Fenichel's normal form theory.

Lemma 4.8. *Let $c \in (0,1)$ and set $\Lambda_2 = \{U_2 | r_2 = \nu\}$. Then as $\epsilon \to 0$, for ν and ρ sufficiently small, the forward flow of $z_2(\epsilon)$ in (4.20) intersects Λ_2 in*

$$\left\{ \Lambda_2 |\ w_2 = -\lambda_+ + \mathcal{O}(\epsilon^c),\ \theta = \theta_0 + \mathcal{O}(\epsilon \ln \epsilon^{-1}),\ \phi = \phi_0 - \frac{c_+(\theta_0)}{p_+(\theta_0)}\lambda_+(\theta_0)\nu + \mathcal{O}(\epsilon^c), \right.$$
$$\left. v = v_0 - \frac{q_+(\theta_0)}{p_+(\theta_0)}\lambda_+(\theta_0)\nu + \mathcal{O}(\epsilon^c) \right\}. \tag{4.22}$$

Proof. By Fenichel's normal form theory, we can straighten out stable and unstable fibres.

Lemma 4.9. *For ν and ρ sufficiently small, then within U_2 there exists a smooth transformation $(\epsilon_2, w_2, \phi, v, r_2) \mapsto (\tilde{\phi}, \tilde{v})$ satisfying*

$$\left.\begin{aligned} \tilde{\phi} &= \phi + \frac{c_+(\theta)}{p_+(\theta)}\lambda_+(\theta) r_2 + \mathcal{O}(r_2(w_2 + \lambda_+)) \\ \text{and} \qquad \tilde{v} &= v + \frac{q_+(\theta)}{p_+(\theta)}\lambda_+(\theta) r_2 + \mathcal{O}(r_2(w_2 + \lambda_+) + \epsilon), \end{aligned}\right\} \tag{4.23}$$

which transforms (4.19) into

$$\left.\begin{aligned} &\epsilon_2' = \epsilon_2 w_2, \quad w_2' = \epsilon_2 b(\theta, \tilde{\phi}) + p_+(\theta)(1 - \delta w_2) + w_2^2 + \mathcal{O}(\epsilon), \\ &\theta' = \epsilon\tilde{\phi}, \quad \tilde{\phi}' = 0, \\ &\tilde{v}' = 0 \quad \text{and} \quad r_2' = -r_2 w_2. \end{aligned}\right\} \tag{4.24}$$

Proof. Replace r_2 by νr_2 in (4.19) and consider ν small. Using $\epsilon = \epsilon_2 r_2$, this brings the system into a classical slow–fast system for $0 < \nu \ll 1$, where (ϵ_2, w_2, r_2) are fast variables while (θ, ϕ, v) are slow. In particular, $\epsilon_2 = r_2 = 0$, $w_2 = -\lambda_+$ is a saddle-type slow manifold for ν small. The system is therefore amenable to Fenichel's normal form theory [33]. The result then follows by returning to the original r_2 and using $\phi = \tilde{\phi} + \mathcal{O}(r_2)$ together with $r_2\epsilon_2 = \epsilon$ in the w_2 equation. ∎

To prove lemma 4.8, we then integrate the normal form (4.24) with initial conditions $z_2(\epsilon)$ from (4.20) from (a reset) time $\tau = 0$ up to $\tau = T$, defined implicitly by $r_2(T) = \nu$. Clearly, $\theta(T) = \theta_0 + \mathcal{O}(\epsilon T)$, $\tilde{\phi}(T) = \tilde{\phi}_0$ and $\tilde{v}(T) = \tilde{v}_0$. Then, from (4.12), Gronwall's inequality and the fact that $1 - \lambda_-\lambda_+^{-1} > 1$, we find

$$\left.\begin{aligned} T &= \lambda_+^{-1} \ln \epsilon^{-1}(1 + o(1)) \\ \text{and} \qquad w_2(T) &= -\lambda_+(1 + \mathcal{O}(e^{-\lambda_+ T} + e^{(\lambda_- - \lambda_+)T} + \epsilon)) \\ &= -\lambda_+ + \mathcal{O}(\epsilon^{c(1-\lambda_-\lambda_+^{-1})} + \epsilon^c) = -\lambda_+ + \mathcal{O}(\epsilon^c), \end{aligned}\right\} \tag{4.25}$$

for $c \in (0,1)$. Then, we obtain the expressions for $\theta = \theta(T)$, $\phi = \phi(T)$ and $v = v(T)$ in (4.22) from (4.23) in terms of the original variables. ∎

(iv) Completing the proof of proposition 4.4

To complete the proof of proposition 4.4, we then return to (4.3) using (4.11) and integrate initial conditions (4.22) within $\{\hat{y} = -r_2 = -\nu\}$, up to the switching manifold $\Sigma = \{v = 0\}$, using regular perturbation theory and the implicit function theorem. This gives (4.9), which completes the proof of proposition 4.4.

(c) Sticking

After the slipping compression phase of the previous section, the rod then sticks on Σ, with $(\hat{y}, w, \theta, \phi)$ given by (4.9). This is a corollary of the following lemma.

Lemma 4.10. *Suppose $a \neq 0$, $q_+ < 0$, $q_- > 0$. Consider the (negative) function*

$$\mathcal{F}(\theta,\phi) = \begin{cases} \dfrac{a(\theta,\phi)}{q_+(\theta)} & \text{if } a > 0, \\ \dfrac{a(\theta,\phi)}{q_-(\theta)} & \text{if } a < 0. \end{cases}$$

Then there exists a set of visible folds at

$$\Gamma_\epsilon \equiv \{(\hat{y}, w, \theta, \phi, v) \in \Sigma |\ \hat{y} + \delta w = \epsilon \mathcal{F}(\theta,\phi)\}, \tag{4.26}$$

of the Filippov system (4.3), dividing the switching manifold $\Sigma : v = 0$ into (stable) sticking: $\Sigma_s \equiv \{(\hat{y}, w, \theta, \phi, v) \in \Sigma |\ \hat{y} + \delta w < \epsilon \mathcal{F}(\theta,\phi)\}$, and crossing upwards (downwards) for $a > 0$ ($a < 0$): $\Sigma_c \equiv \{(\hat{y}, w, \theta, \phi, v) \in \Sigma |\ \hat{y} + \delta w > \epsilon \mathcal{F}(\theta,\phi)\}$.

Proof. Simple computations, following [4]; see also proposition 2.1. ∎

The forward motion of (4.9) within $\Sigma_s \subset \Sigma$ for $\epsilon \ll 1$ is therefore subsequently described by the Filippov vector-field (2.8) in proposition 2.1,

$$\left.\begin{aligned} &\hat{y}' = w, \quad w' = \epsilon b(\theta,\phi) + S_w(\theta)[-\hat{y} - \delta w], \\ &\theta' = \epsilon\phi \quad \text{and} \quad \phi' = S_\phi(\theta)[-\hat{y} - \delta w], \end{aligned}\right\} \tag{4.27}$$

here written in terms of $\hat{y}$ and the fast time τ, until sticking ends at the visible fold Γ_ϵ. Note this always occurs for $0 < \epsilon \ll 1$ since $\hat{y}'' = w' > 0$, for $[-\hat{y} - \delta w] > 0$.

We first focus on $\epsilon = 0$. From (4.27), $\theta = \theta_0$, a constant, and

$$\left.\begin{aligned} &\hat{y}' = w, \\ &w' = S_w(\theta)[-\hat{y} - \delta w] \\ \text{and} \qquad &\phi' = S_\phi(\theta)[-\hat{y} - \delta w]. \end{aligned}\right\} \tag{4.28}$$

We now integrate (4.28), using (4.9) for $\epsilon = 0$ as initial conditions, given by

$$(\hat{y}(0), w(0), \phi(0)) = \left(-\frac{p_+(\theta_0)}{q_+(\theta_0)\lambda_+(\theta_0)} v_0, -\frac{p_+(\theta_0)}{q_+(\theta_0)} v_0, \phi_0 - \frac{c_+(\theta_0)}{q_+(\theta_0)} v_0 \right), \tag{4.29}$$

up until the section $\Gamma_0 : \hat{y} + \delta w = 0$ shown in figure 3*a*, where sticking ceases for $\epsilon = 0$, by lemma 4.10 and $(4.26)_{\epsilon=0}$. We then obtain a function $e(\delta, \theta_0) > 0$ in the following proposition, which relates the horizontal velocity at the start of the slipping compression phase v_0 (3.1) with the values of $(\hat{y}, w, \phi)$ on Γ_0, at the end of the sticking phase.

Proposition 4.11. *There exists a smooth function $e(\delta, \theta_0) > 0$ and a time $\tau_s > 0$ such that $(\hat{y}(\tau_s), w(\tau_s), \phi(\tau_s)) \in \Gamma_0$ with*

$$\left.\begin{aligned} &\hat{y}(\tau_s) = -\delta e(\delta, \theta_0) v_0, \\ &w(\tau_s) = e(\delta, \theta_0) v_0 \\ \textit{and} \qquad &\phi(\tau_s) = \phi_0 + \left\{ -\frac{c_+(\theta_0)}{q_+(\theta_0)} + \frac{S_\phi(\theta_0)}{S_w(\theta_0)} \left(e(\delta, \theta_0) + \frac{p_+(\theta_0)}{q_+(\theta_0)} \right) \right\} v_0, \end{aligned}\right\}$$

where $(\hat{y}(\tau), w(\tau), \phi(\tau))$ is the solution of (4.28) with initial conditions (4.29). The function $e(\delta, \theta_0)$ is monotonic in δ: $\partial_\delta e(\delta, \theta_0) < 0$, and satisfies (3.4) and (3.5) for $\delta \gg 1$ and $\delta \ll 1$, respectively.

Proof. The existence of τ_s is obvious. Linearity in v_0 follows from (4.29) and the linearity of (4.28) within $\hat{F}_N > 0$. Since $\dot{\hat{y}} = w$, we have $e > 0$. The ϕ equation follows since $\phi' = w' S_\phi(\theta)/S_w(\theta)$. The monotonicity of e as a function δ is the consequence of simple arguments in the $(w, \hat{y})$-plane using (4.28) and the fact that $w(0)$ in (4.29) is independent of δ while $\hat{y}(0) = \hat{y}_0(\delta)$ decreases (since λ_+ is an increasing function of δ). To obtain the asymptotics, we first solve (4.28) with

$\delta \neq 2/\sqrt{S_w(\theta_0)}$. Simple calculations show that

$$e(\delta, \theta_0) = \frac{\xi_+}{\xi_-}(\lambda_+ - \xi_-)\frac{p_+}{q_+\lambda_+}e^{\xi_+\tau_s}, \tag{4.30}$$

suppressing the dependency on θ_0 on the right-hand side, where $\xi_\pm = -\delta S_w/2 \pm \frac{1}{2}\sqrt{\delta^2 S_w^2 - 4S_w}$ and τ_s is the least positive solution of $e^{(\xi_+-\xi_-)\tau_s} = \xi_-^2(\lambda_+ - \xi_+)/\xi_+^2(\lambda_+ - \xi_-)$. For $\delta \gg 1$, the eigenvalues $\xi_\pm$ are real and negative. Hence, $\tau_s = 1/(\xi_+ - \xi_-)\ln(\xi_-^2(\lambda_+ - \xi_+)/\xi_+^2(\lambda_+ - \xi_-))$. Now using $\xi_+ = -S_w\delta(1 + \mathcal{O}(\delta^{-2}))$, $\xi_- = S_w/\xi_- = -\delta^{-1}(1 + \mathcal{O}(\delta^{-1}))$, and $\lambda_+ = -p_+\delta(1 + \mathcal{O}(\delta^{-2}))$, we obtain $\xi_+\tau_s = \mathcal{O}(\delta^{-2}\ln\delta^{-1})$, and hence

$$e(\delta, \theta_0) = -\frac{S_w - p_+}{q_+ S_w}\delta^{-2}(1 + \mathcal{O}(\delta^{-2}\ln\delta^{-1})), \tag{4.31}$$

as $\delta \to \infty$. For $\delta \ll 1$, $\xi_\pm$ are complex conjugated with negative real part. This gives $\tau_s = (2i/(\xi_+ - \xi_-))(\chi - \pi n)$, $\chi = \arg((\lambda_+ - \xi_+)\xi_-^2) > 0$, $n = \lfloor \chi/\pi \rfloor$. Using the asymptotics of $\xi_\pm$ and λ_+, we obtain $\tau_s = (\pi - \arctan(\sqrt{-S_w/p_+}))/\sqrt{S_w} - \frac{1}{2}\delta(1 + \mathcal{O}(\delta))$, and then

$$e(\delta, \theta_0) = -\frac{\sqrt{p_+(p_+ - S_w)}}{q_+}\left(1 - \frac{\sqrt{S_w}}{2}\left(\pi - \arctan\left(\sqrt{-\frac{S_w}{p_+}}\right)\right)\delta + \mathcal{O}(\delta^2)\right), \tag{4.32}$$

as $\delta \to 0^+$. Simple algebraic manipulations of (4.31) and (4.32) using (2.9) give the expressions in (3.4) and (3.5). ■

Remark 4.12. The critical value $\delta = \delta_{\text{crit}}(\theta_0) \equiv 2/\sqrt{S_w(\theta_0)}$ gives a double root of the characteristic equation. For the classical Painlevé problem, $\delta_{\text{crit}}(\pi/2) = 2$, as expected (see §2b).

For $0 < \epsilon \ll 1$, sticking ends along the visible fold at Γ_ϵ. We therefore perturb from $\epsilon = 0$ as follows:

Proposition 4.13. *The forward flow of* (4.9) *under the Filippov vector-field* (4.27) *intersects the set of visible folds* Γ_ϵ $o(1)$*-close to the intersection of* $(4.9)_{\epsilon=0}$ *with* Γ_0 *described in proposition* 4.11.

Proof. Since the $\epsilon = 0$ system is transverse to Γ_0, we can apply regular perturbation theory and the implicit function theorem to perturb τ_s continuously to $\tau_s + o(1)$. The result then follows. ■

(d) Lift-off

Beyond Γ_ϵ we have $\hat{F}_N \equiv 0$ and lift-off occurs. For $\epsilon = 0$, we have $\hat{y}' = w$ and $w' = \theta' = \phi' = v' = 0$. By proposition 4.13 and regular perturbation theory, we obtain the desired result in theorem 3.1. In terms of the original (slow) time t, it follows that the time of IWC is of order $\mathcal{O}(\epsilon\ln\epsilon^{-1})$ (recall (4.25)). As $\epsilon \to 0$, IWC occurs instantaneously.

5. Proof of theorem 3.2: impact without collision in the indeterminate case

Here, by assumption (3.7), we have $b > 0$. Therefore, we have, using $p_+ < 0$, that $C_1 = \{\hat{y}_1 = b/p_+, w_1 = 0\} \subset \{\hat{y}_1 < 0\}$ is a critical set of $(4.15)_{\epsilon=0}$; see also figure 5. The stable manifold of $C_1 \cap \{\theta = \theta_0, \phi = \phi_0, v = v_0\}$ within $\hat{y} \leq 0$ is

$$\gamma_1^s(\theta_0, \phi_0, v_0) = \left\{(\hat{y}_1, w_1, \theta_0, \phi_0, v_0) |\ w_1 = \lambda_-(\theta_0)\left(\hat{y}_1 - \frac{b(\theta_0, \phi_0)}{p_+(\theta_0)}\right),\ \hat{y}_1 \leq 0\right\}, \tag{5.1}$$

recall (4.5), with λ_- defined in (4.6). γ_1^s therefore intersects the w_1-axis in

$$\gamma_1^s \cap \{\hat{y}_1 = 0\}:\ w_1 = w_{1*} \equiv -\lambda_-(\theta_0)\frac{b(\theta_0, \phi_0)}{p_+(\theta_0)} < 0, \tag{5.2}$$

and divides the negative w_1-axis into (i) initial conditions that lift off directly ($w_{10} > w_{1*}$, dotted cyan in figure 5) and (ii) initial conditions that undergo IWC before returning to $\hat{y} = 0$ ($w_{10} < w_{1*}$, purple in figure 5). (A canard phenomenon occurs around $w_{10} = w_{1*}$ for $0 < \epsilon \ll 1$, where the

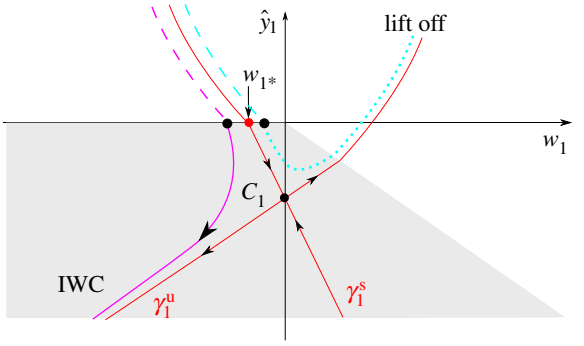

Figure 5. Phase portrait (4.15)$_{\epsilon=0}$ for $b > 0$ (theorem 3.2 in §5). Here, $C_1 = \{\hat{y}_1 = b/p_+, w_1 = 0\}$ is a saddle-type critical manifold for the PWS system, γ_1^u is given by (4.16), γ_1^s by (5.1) and w_{1*} by (5.2). As in figure 4, the grey region is where $\hat{F}_{N,1} > 0$. Orbit segments outside this region are parabolas. Dashed lines indicate backward orbits, from initial conditions on the w_1-axis. A similar figure appears in [6].

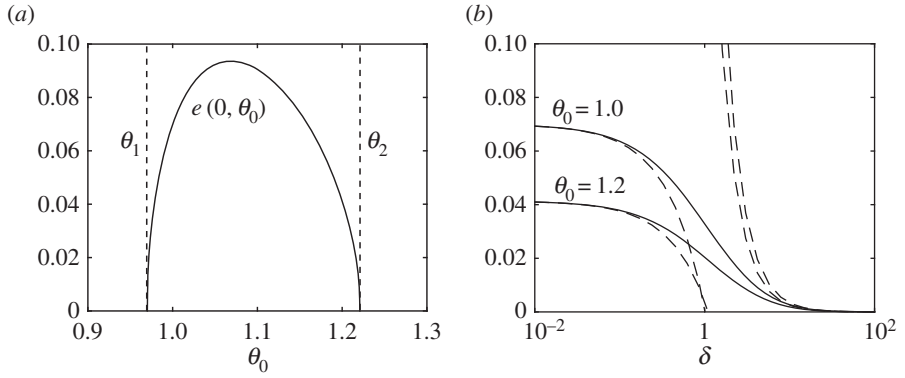

Figure 6. (*a*) Graph of $e(0, \theta_0)$ from (6.2), where $\theta_{1,2}$ are given by (2.14). (*b*) Graph of $e(\delta, \theta_0)$ for $\theta_0 = 1$ and $\theta_0 = 1.2$, where the dashed lines correspond to the approximations obtained from (3.4) and (3.5). For both figures, $\alpha = 3$ and $\mu = 1.4$.

solution follows a saddle-type slow manifold for an extended period of time.) In theorem 3.2, we consider $w_{10} < w_{1*}$. The remainder of the proof of theorem 3.2 on IWC in the indeterminate case then follows the proof of theorem 3.1.

6. Discussion

The quantity $e(\delta, \theta_0)$ in theorems 3.1 and 3.2 relates the initial horizontal velocity v_0 of the rod to the resulting vertical velocity at the end of IWC. It is like a 'horizontal coefficient of restitution'. The leading order expression of $e(\delta, \theta_0)$ in (3.4) for $\delta \gg 1$ is independent of μ, in general. Using the expressions for $q_\pm$ and $p_\pm$ in (2.6), together with (4.31), we find for large δ that

$$e(\delta, \theta_0) = \frac{\alpha}{2(1+\alpha)} \sin(2\theta_0)\delta^{-2}(1 + \mathcal{O}(\delta^{-2} \ln \delta^{-1})), \quad \theta_0 \in (\theta_1, \theta_2). \tag{6.1}$$

The limit $\delta \to \infty$ is not uniform in $\theta \in (\theta_1, \theta_2)$.

The expression for $\delta \ll 1$ is more complicated and *does* depend upon μ, in general. Using (2.6) and (4.32), for $\delta = 0$, we have

$$e(0, \theta_0) = \sqrt{\frac{(1 + \alpha\cos^2\theta_0 - \mu\alpha \sin\theta_0 \cos\theta_0)}{(\alpha \sin\theta_0 \cos\theta_0 - \mu(1 + \alpha \sin^2\theta_0))} \frac{\alpha \sin\theta_0 \cos\theta_0}{(1 + \alpha \sin^2\theta_0)}}. \tag{6.2}$$

We plot $e(0, \theta_0)$ in figure 6*a* for $\alpha = 3$ and $\mu = 1.4$. Figure 6*b* shows the graph of $e(\delta, 1)$ and $e(\delta, 1.2)$ along with the approximations (dashed lines) in (3.4) and (3.5).

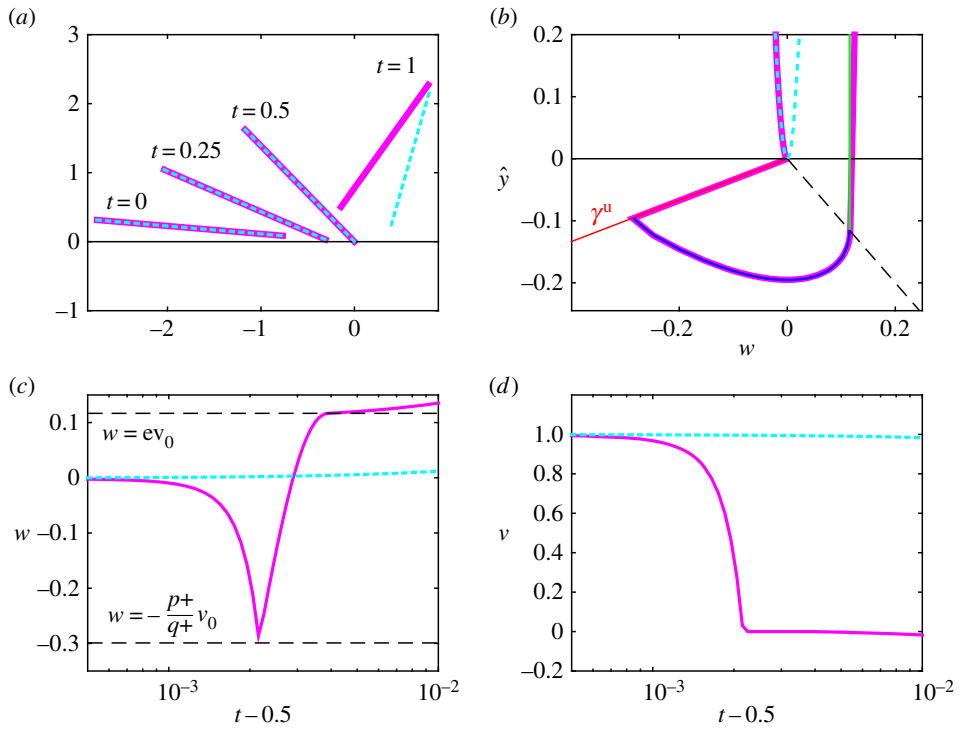

Figure 7. (*a*) Dynamics of the Painlevé rod described by the Filippov system (2.5) for $\mu = \alpha = 3$, $\delta = 1$ and $\epsilon = 10^{-3}$ in the indeterminate case. The purple and cyan rods are separated at $t = 0$ by a distance of 10^{-3}. At around $t = 0.5$, impact with the compliant surface occurs. The purple rod experiences IWC, whereas the cyan rod lifts off directly. (*b*) Projection onto the $(w, \hat{y})$-plane. The blue sticking orbit and the green lift-off orbit from figure 3*b* are also shown. The numerical and theoretical results are indistinguishable. (*c*,*d*) w and v as functions of time near $t = 0.5$ for both rods.

In the inconsistent case, described by theorem 3.1, the initial conditions (3.1) are very similar to those assumed by [24]. Interestingly, by applying the approach in §4b backwards in time, it follows that the backward flow of (3.1) for $b < 0$ (dashed lines in figure 4, illustrating the κ_1 dynamics) follows γ^s, the stable manifold of C for $\epsilon = 0$, as $\epsilon \to 0$. Hence, by $(4.3)_{\epsilon=0}$, the horizontal velocity v (and therefore also the energy) increases unboundedly. This 'backward blowup' occurs on the fast time-scale τ. As a consequence, it is impossible to set up the conditions (3.1) in an experiment without using some form of controller (as was done in [15] for the two-link manipulator system).

The indeterminate case, described by theorem 3.2, is characterized by an extreme exponential splitting in phase space, due to the stable manifold of C_1 in the κ_1 system. For example, the cyan orbit in figure 5 lifts off directly with $w = \mathcal{O}(\epsilon)$. But on the other side of the stable manifold, the purple orbit undergoes IWC and then lifts off with $w = \mathcal{O}(1)$. The initial conditions in theorem 3.2 correspond to orbits that are almost grazing ($\dot{y} = w = \mathcal{O}(\epsilon)$, $\ddot{y} = \dot{w} = b > 0$) the compliant surface at $y = 0$. In figure 7, we illustrate this further by computing the full Filippov system $(2.5)_{\epsilon=10^{-3}}$ for two rods (purple and cyan as in figure 5) initially distant by an amount of 10^{-3} above the compliant surface ($y \approx 0.1$, see also $t = 0$ in figure 7*a*). We set $\mu = \alpha = 3$, $\delta = 1$. Figure 7*a* shows the configuration of the rods at different times $t = 0$, $t = 0.25$, $t = 0.5$ and $t = 1$. Up until $t = 0.5$, the two rods are indistinguishable. At $t = 0.5$, grazing ($\dot{y} = w \approx -10^{-3}$) with the compliant surface $y = 0$ occurs where $\theta \approx 0.9463$, $\phi \approx 1.6654$, and $v \approx 1.00$ (so $b \approx 1.2500$ and $p_+ \approx -2.243$). The purple rod then undergoes IWC, occurring on the fast time-scale τ, and therefore subsequently lifts off from $y = 0$ with $w = \mathcal{O}(1)$. In comparison, the cyan rod lifts off with $w \approx 10^{-3}$. At $t = 1$, the two rods are clearly separated. Figure 7*b* shows the projection of the numerical solution in figure 7*a* onto the

$(w, \hat{y})$-plane, together with the theoretical predictions of figure 3*b*. Note that the numerical and analytical solutions are indistinguishable, in both the sticking and lift-off regimes. The cyan orbit lifts off directly. The purple orbit, being on the other side of the stable manifold of C_1, follows the unstable manifold (γ_u, shown in red) until sticking occurs. Then when $\hat{F}_N = 0$ at $\hat{y} + \delta\hat{w} = 0$ (dashed line), lift-off occurs almost vertically in the $(w, \hat{y})$-plane. Figure 7*c*,*d* shows the vertical velocity w and horizontal velocity v, respectively, for both orbits over the same time interval as figure 7*b*; note the sharp transition for the purple orbit around $t = 0.5$, as it undergoes IWC. In figure 7*c*, we include two dashed lines $w = ev_0$ and $w = -(p_+/q_+)v_0$, corresponding to our analytical results (3.3) and (4.9), which also hold for the indeterminate case (from theorem 3.2), in excellent agreement with the numerical results.

7. Conclusion

We have considered the problem of a rigid body, subject to a unilateral constraint, in the presence of Coulomb friction. Our approach was to regularize the problem by assuming a compliance with stiffness and damping at the point of contact. This leads to a slow–fast system, where the small parameter ϵ is the inverse of the square root of the stiffness.

Like other authors, we found that the fast time-scale dynamics is unstable. Dupont & Yamajako [21] established conditions in which these dynamics can be stabilized. By contrast, McClamroch [28] established under what conditions the unstable fast time-scale dynamics could be controlled by the slow time-scale dynamics. Other authors have used the initial scaling (4.1), together with the scaling κ_1 to numerically compute stability boundaries [21,28] or phase plane diagrams [6].

The main achievement of this paper is to rigorously derive these, and other, results that have eluded others in simpler settings. For example, the work of Zhao *et al.* [24] assumes no damping in the compliance and uses formal methods to provide estimates of the times spent in the three phases of IWC. They suggest that their analysis can '$\cdots$ roughly explain why the Painlevé paradox can result in [IWC]'. By contrast, we assumed that the compliance has *both* stiffness and damping, analysed the problem rigorously, derived exact and asymptotic expressions for many important quantities in the problem and showed *exactly* how and why the Painlevé paradox can result in IWC. There are no existing results comparable to (3.3)–(3.5) for any value of δ.

Our results are presented for arbitrary values of the compliance damping, and we are able to give explicit asymptotic expressions in the limiting cases of small and large damping, all for a large class of rigid bodies, including the case of the classical Painlevé example in figure 1.

Given a general class of rigid body and a general class of normal reaction, we have been able to derive an explicit connection between the initial horizontal velocity of the body and its lift-off vertical velocity, for arbitrary values of the compliance damping, as a function of the initial orientation of the body.

Authors' contributions. S.J.H. and K.U.K. wrote the paper and carried out the calculations at DTU during August and September 2016. Subsequently, K.U.K. carried out the numerical simulations, following referees' comments. Both authors gave final approval for publication.

Competing interests. We have no competing interests.

Funding. S.J.H. was partly supported by EPSRC grant no. EP/I013717/1.

References

1. Painlevé P. 1895 Sur les loi du frottement de glissement. *C. R. Seances Acad. Sci.* **121**, 112–115.
2. Painlevé P. 1905 Sur les loi du frottement de glissement. *C. R. Seances Acad. Sci.* **141**, 401–405.
3. Painlevé P. 1905 Sur les loi du frottement de glissement. *C. R. Seances Acad. Sci.* **141**, 546–552.
4. Filippov AF. 1988 *Differential equations with discontinuous righthand sides*. Mathematics and its applications. Dordrecht, The Netherlands: Kluwer Academic Publishers.
5. Brogliato B. 1999 *Nonsmooth mechanics*, 2nd edn. London, UK: Springer.
6. Champneys AR, Várkonyi P. 2016 The Painlevé paradox in contact mechanics. *IMA J. Appl. Math.* **81**, 538–588. (doi:10.1093/imamat/hxw027)

7. Shen Y, Stronge WJ. 2011 Painlevé's paradox during oblique impact with friction. *Eur. J. Mech. A Solids* **30**, 457–467. (doi:10.1016/j.euromechsol.2011.03.001)
8. Stewart DE. 2000 Rigid-body dynamics with friction and impact. *SIAM Rev.* **42**, 3–39. (doi:10.1137/S0036144599360110)
9. Leine R, Brogliato B, Nijmeijer H. 2002 Periodic motion and bifurcations induced by the Painlevé paradox. *Eur. J. Mech. A Solids* **21**, 869–896. (doi:10.1016/S0997-7538(02)01231-7)
10. Liu C, Zhao Z, Chen B. 2007 The bouncing motion appearing in a robotic system with unilateral constraint. *Nonlinear Dyn.* **49**, 217–232. (doi:10.1007/s11071-006-9123-z)
11. Neimark YI, Fufayev NA. 1995 The Painlevé paradoxes and the dynamics of a brake shoe. *J. Appl. Math. Mech.* **59**, 343–352. (doi:10.1016/0021-8928(95)00041-M)
12. Or Y. 2014 Painlevé's paradox and dynamic jamming in simple models of passive dynamic walking. *Regul. Chaotic Dyn.* **19**, 64–80. (doi:10.1134/S1560354714010055)
13. Or Y, Rimon E. 2012 Investigation of Painlevé's paradox and dynamic jamming during mechanism sliding motion. *Nonlinear Dyn.* **67**, 1647–1668. (doi:10.1007/s11071-011-0094-3)
14. Wilms EV, Cohen H. 1981 Planar motion of a rigid body with a friction rotor. *ASME J. Appl. Mech.* **48**, 205–206. (doi:10.1115/1.3157576)
15. Zhao Z, Liu C, Ma W, Chen B. 2008 Experimental investigation of the Painlevé paradox in a robotic system. *ASME J. Appl. Mech.* **75**, 041006. (doi:10.1115/1.2910825)
16. Lecornu L. 1905 Sur la loi de Coulomb. *C. R. Seances Acad. Sci.* **140**, 847–848.
17. Génot F, Brogliato B. 1999 New results on Painlevé paradoxes. *Eur. J. Mech. A Solids* **18**, 653–677. (doi:10.1016/S0997-7538(99)00144-8)
18. Ivanov AP. 1986 On the correctness of the basic problem of dynamics in systems with friction. *J. Appl. Math. Mech.* **50**, 547–550. (doi:10.1016/0021-8928(86)90026-2)
19. Darboux G. 1880 Étude géometrique sur les percussions et le choc des corps. *Bull. Sci. Math. Astron. 2e Ser.* **4**, 126–160.
20. Keller JB. 1986 Impact with friction. *ASME J. Appl. Mech.* **53**, 1–4. (doi:10.1115/1.3171712)
21. Dupont PE, Yamajako SP. 1997 Stability of frictional contact in constrained rigid-body dynamics. *IEEE Trans. Robot. Autom.* **13**, 230–236. (doi:10.1109/70.563645)
22. Song P, Kraus P, Kumar V, Dupont PE. 2001 Analysis of rigid-body dynamic models for simulation of systems with frictional contacts. *ASME J. Appl. Mech.* **68**, 118–128. (doi:10.1115/1.1331060)
23. An LS. 1990 The Painlevé paradoxes and the law of motion of mechanical systems with Coulomb friction. *J. Appl. Math. Mech.* **54**, 430–438. (doi:10.1016/0021-8928(90)90052-C)
24. Zhao Z, Liu C, Chen B, Brogliato B. 2015 Asymptotic analysis and Painlevé's paradox. *Multibody Syst. Dyn.* **35**, 299–319. (doi:10.1007/s11044-014-9448-1)
25. Neimark YI, Smirnova VN. 2001 Contrast structures, limit dynamics and the Painlevé paradox. *Differ. Equ.* **37**, 1580–1588. (doi:10.1023/A:1017916832078)
26. Uldall Kristiansen K, Hogan SJ. 2015 On the use of blowup to study regularizations of singularities of piecewise smooth dynamical systems in $\mathbb{R}^3$. *SIAM. J. Appl. Dyn. Syst.* **14**, 382–422. (doi:10.1137/140980995)
27. Uldall Kristiansen K, Hogan SJ. 2015 Regularizations of two-fold bifurcations in planar piecewise smooth systems using blowup. *SIAM. J. Appl. Dyn. Syst.* **14**, 1731–1786. (doi:10.1137/15M1009731)
28. McClamroch NH. 1989 A singular perturbation approach to modeling and control of manipulators constrained by a stiff environment. In *Proc. 28th Conf. on Decision and Control, Tampa, FL, 13–15 December*, pp. 2407–2411. Piscataway, NJ: IEEE.
29. Uldall Kristiansen K, Hogan SJ. 2017 Le canard de Painlevé. (http://arxiv.org/abs/1703.07665)
30. Fenichel N. 1971 Persistence and smoothness of invariant manifolds for flows. *Indiana Univ. Math. J.* **21**, 193–226. (doi:10.1512/iumj.1972.21.21017)
31. Fenichel N. 1974 Asymptotic stability with rate conditions. *Indiana Univ. Math. J.* **23**, 1109–1137. (doi:10.1512/iumj.1974.23.23090)
32. Fenichel N. 1979 Geometric singular perturbation theory for ordinary differential equations. *J. Differ. Equ.* **31**, 53–98. (doi:10.1016/0022-0396(79)90152-9)
33. Jones CKRT. 1995 *Geometric singular perturbation theory*. Lecture Notes in Mathematics, Dynamical Systems (Montecatini Terme). Berlin, Germany: Springer.
34. Kuehn C. 2015 *Multiple time scale dynamics*. Berlin, Germany: Springer.
35. Krupa M, Szmolyan P. 2001 Extending geometric singular perturbation theory to nonhyperbolic points—fold and canard points in two dimensions. *SIAM J. Math. Anal.* **33**, 286–314. (doi:10.1137/S0036141099360919)